In: Magnetic Properties of Solids
Editor: Kenneth B. Tamayo, pp. 179-202

ISBN: 978-1-60741-550-3

Chapter 4

PROCESSING AND PROPERTIES OF THIN MANGANITE FILMS

S. Canulescu[1], C.N. Borca[2], M. Döbeli[3], P. Schaaf[4], T. Lippert[2] and A. Wokaun[2]

[1] EMPA Materials Science and Technology, CH-3602 Thun, Switzerland
[2] Paul Scherrer Institut, CH-5232 Villigen, Switzerland
[3] Ion Beam Physics, Paul Scherrer Institut and ETH Zurich, CH-8093 Zurich, Switzerland
[4] TU Ilmenau, Institute of Materials Engineering and Institute of Micro- and Nanotechnologies, D-98684 Ilmenau, Germany

Abstract

The perovskite- type compounds $RE_{1-x}M_xMnO_3$ (RE= rare earth, M = Ca, Sr, Ba, Pb) exhibit remarkable electronic and transport properties induced by the presence of mixed Mn^{3+}/Mn^{4+} valence states. In particular, mixed valence perovskites have been extensively studied due to their spectacular colossal magnetoresistance (CMR) effect. The most important features of the CMR manganites are reviewed. Here we present our findings on $La_{0.7}Ca_{0.3}Mn_{1-x}Fe_xO_3$ (x=0 and 0.2) thin films grown by Pulsed Reactive Crossed Beam Laser Ablation. The structural, electronic and transport properties of the films were determined and correlated with the growth parameters. The influence of the oxygen vacancies on the transport properties of the $La_{0.7}Ca_{0.3}MnO_3$ thin films, and in particular on the colossal magnetoresistance effect is discussed. Changes in the manganese valence states monitored by means of the X-ray photoelectron spectroscopy (as surface sensitive technique) and X- ray absorption spectroscopy technique (as bulk sensitive technique) are correlated with the transport properties of the thin films (bulk resistivity and magnetoresistance).

Fe doping (20%) on Mn sites induces changes in the transport properties of $La_{0.7}Ca_{0.3}Mn_{0.8}Fe_{0.2}O_3$ thin films. A considerable decrease in the colossal magnetoresistance value after Fe doping is reported. X- ray absorption spectroscopy measurements for the Fe-sites in these compounds indicate an increased localization of the Mn e_g orbitals upon Fe substitution, which weakens the double exchange interaction. The importance of the double exchange interaction on the magnetoresistance effect is extensively discussed.

Introduction

Future electronic technologies, i.e. spintronics, would like to take advantage of the electrons spin degree of freedom (with its orientation up or down), in addition to its charge, in order to store or transmit information.

The giant magnetoresistance (GMR) was first reported in Fe/Co multilayers in 1988 [1] and rapidly applied in reading heads for hard drives. In GMR materials, a weak magnetic field is applied to align the spin of electrons, inducing a large change in the electrical resistance of the material.

One decade later, a change of the bulk resistivity by several orders of magnitude was reported in the manganite system, termed "colossal magnetoresistance" effect (CMR). Von Helmholt *et al.* reported a magnetoresistance of about 60% in $La_{0.67}Ba_{0.33}MnO_3$ [2], and M. McCormack *et al.* measured a magnetoresistance of the La-Ca-Mn-O layers that exceeded 99.92% at 77 K [3].

Due to the remarkable interrelated structural, magnetic and transport properties, the CMR materials have fueled a lot of enthusiasm in research, as well as technological interest. During the attempts to understand the physics of the CMR, many interesting properties of the manganites have been observed, such as charge ordering, phase separation, and half metallicity. The mixed-valence perovskites $RE_{1-x}M_xMnO_3$ (RE= rare earth, M = Ca, Sr, Ba, Pb) show an antiferromagnetic (AF) insulating behavior (at low and large x values) and ferromagnetic (F) metallic behavior for a value around $x \sim 1/3$ [4,5]. The parent compound of the CMR manganites is an antiferromagnetic $LaMnO_3$ material, with an orthorhombic structure. The partial substitution of the trivalent La ions by divalent ions, such as Ca, Sr, Ba, results in the formation of CMR materials, with a composition of $La_{1-x}M_xMnO_3$ (M = Ca, Sr, Ba, Pb). The CMR compound has mixed Mn^{3+}/Mn^{4+} valence states, where the Mn^{4+} concentration is proportional with the divalent ion substitution. The conduction mechanism in manganites is determined by the transfer of e_g electrons from Mn^{3+} to Mn^{4+} via the double exchange (DE) interaction [6]. The e_g electrons become delocalized in the ferromagnetic phase for a certain range of doping centered around $x \approx 1/3$ and a FM state is established at low temperature.[1].

In addition to the double- exchange interaction that promotes hopping of carriers, Jahn-Teller splitting of the outer Mn 3d levels was introduced to give a complementary explanation for the magnetoresistance effect [7]. The distortion of the oxygen octahedra, determined by the presence of the Mn^{3+} Jahn- Teller ions in the perovskite structure, leads to a localization of the carriers in the form of small polarons in the paramagnetic phase. Ahn et al. [8] have shown that Fe doping (<20%) on the Mn site in the ferromagnetic x= 0.37 and the antiferromagnetic x= 0.53 phases of the $La_{1-x}Ca_xMnO_3$ powders leads to a suppression of the ferromagnetism and conduction.

The research was further extended on layered manganites materials, such as $La_{2-2x}Sr_{1+2x}M_2O_7$ [9] and $SrMn_{1-x}Fe_xO_{3-\delta}$ (x= 1/3, 1/2, 2/3) [10]. Larger CMR values for single crystals and thin films were reported. High quality epitaxial films can be prepared by pulsed laser deposition (PLD), which is the most straightforward method for materials with a complex stoichiometry, such as manganite oxides.

In this chapter, we report our findings on the growth of $La_{0.7}Ca_{0.3}Mn_{1-x}Fe_xO_3$ (x=0 and 0.2) thin films by Pulsed Laser Deposition. The aim of this chapter is to emphasize the main

parameters which influence the transport properties of the thin manganite films, e.g. bulk resistivity and magnetoresistance. The growth technique will be shortly reviewed. Studies on the morphological, structural, electronic and electric properties of the $La_{0.7}Ca_{0.3}MnO_3$ thin films are reported. The role of the Mn^{3+} Jahn- Teller ions on the CMR properties of the manganites is studied by replacing part of the Mn ions by Fe ions (20%).

1. Processing of Thin Manganite Films

The properties of the manganites vary considerably from polycrystalline to single crystalline ceramics and/or thin films. Larger magnetoresistance values have been reported for thin films compared to the bulk materials [11]. High quality epitaxial films can be prepared by pulsed laser deposition (PLD), which is a relatively straightforward method for deposition of materials with a complex stoichiometry, such as manganite oxides. Pulsed Laser Deposition (PLD) showed remarkable results for the deposition of high- T_c superconductors [12], nitrides [13], carbides [14], dielectrics [15], and semiconductors [16]. The principle of pulsed laser deposition is simple and versatile: (i) an intense laser beam is focused through an optical window onto a target placed in a vacuum chamber; (ii) above a certain threshold fluence, a luminous plasma arising from the excited species of the ablated material is formed and (iii) the evaporated material will recondense on a substrate which can be placed in an on-axis geometry (perpendicular to the expanding plume) or off- axis (parallel or at an angle to the expanding plume).

For the growth of oxide films, an oxidizing environment is necessary to be maintained during the deposition process in order to form the desired crystal phase at the deposition temperature. One approach to improve the oxygen content in the films was the development of a pulsed reactive crossed beam laser ablation (PRCLA) setup, as shown schematically in figure 1. The main feature of PRCLA is the interaction between the ablated plume and a pulsed gas. The purpose of the pulsed gas valve is mainly to limit the use of the reactive gas when the transfer and deposition of material occurs, but also to provide higher pressure during the interactions, while maintaining a low background pressure. This can be experimentally achieved by using a distance of maximum 1 cm between the nozzle and the ablation point on the target, which results in a strong degree of scattering between the gas and the plume species (see figure 1). After passing the interaction region, the two beams expand almost collisionless into a low background gas (0.1 Pa) while maintaining their reactivity for the film growth [17].

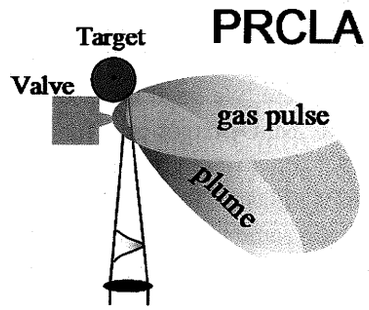

Figure 1. Schematic drawing of a pulsed reactive crossed beam laser ablation configuration.

2. Morphology and Crystalline Quality of $La_{0.7}Ca_{0.3}MnO_3$ Thin Films

2.1. Studies of the Growth Parameters

Reports from conventional PLD reveal that the plume length determines the morphology and microstructure of the growing films. A correlation between the target to substrate distance and substrate temperature which determines the morphology and structural quality of the growing films was found [18]. PLD is a suitable technique for the deposition of complex compounds, providing a stoichiometric transfer of the material; nevertheless, a slight incongruent transfer in the PLD process has been reported [19]. Several factors may account for the incongruent transfer, such as laser fluence, interaction processes in the gas phase, preferential re-sputtering from the deposited films, or thermally- induced processes on the hot substrate. The laser fluence is an experimental parameter which determines the kinetic energy of the plume species and the amount of the evaporated material per pulse. High laser fluence may induce deficiencies of the elements in the growing films due to the bombardment of the film with high energy ions and atoms arising from the ablation process. An incongruent transfer was reported during laser ablation of a FeSiGaRu target, using fluences higher than 6 Jcm^{-2}, due to the preferential sputtering of gallium [20].

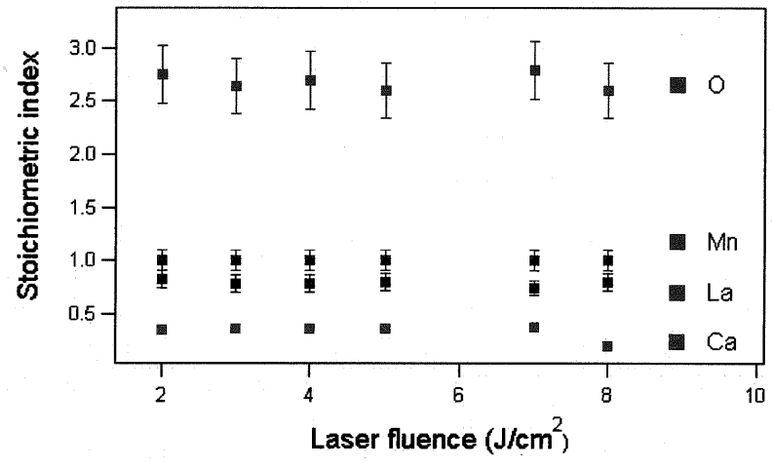

Figure 2. Composition of $La_{0.6}Ca_{0.4}MnO_3$ films deposited at various laser fluences. The relative error is ~5%.

Relevant to the work reported here, we have investigated the elemental composition of the films prepared from a $La_{0.6}Ca_{0.4}MnO_3$ target as a function of the laser fluence, ranging from 2 - 8 Jcm^{-2} (see figure 2). All films were grown on $SrTiO_3$ substrates. According to the Rutherford Back Scattering (RBS)/Elastic Recoil Detection (ERDA) RBS analysis, the composition of the films follows the same trend for a laser fluence ranging from 2 – 7 Jcm^{-2}. For the highest applied fluence (8 Jcm^{-2}) RBS analysis reveals a non- uniform elemental composition through the film. The composition determined by RBS analysis is the average composition over the films thickness. The RBS data indicate a slightly incongruent transfer of

the material, e.g. the growing films are Ca and O deficient. Ca enrichment at the surface (and therefore depletion in bulk) has been previously reported during the growth of the La - Ca - Mn - O films and it was mainly attributed to a surface segregation process [19].

The corresponding average growth rate dependence on the laser fluence, calculated as the ratio between films thickness and the number of pulses, is shown in figure 2. As expected, the growth rate increases with laser fluence. An increase in the laser fluence from 2 - 8 Jcm^{-2} corresponds to an increase of the growth rate from 0.012 Å / pulse to 2.15 Å / pulse (see figure 3).

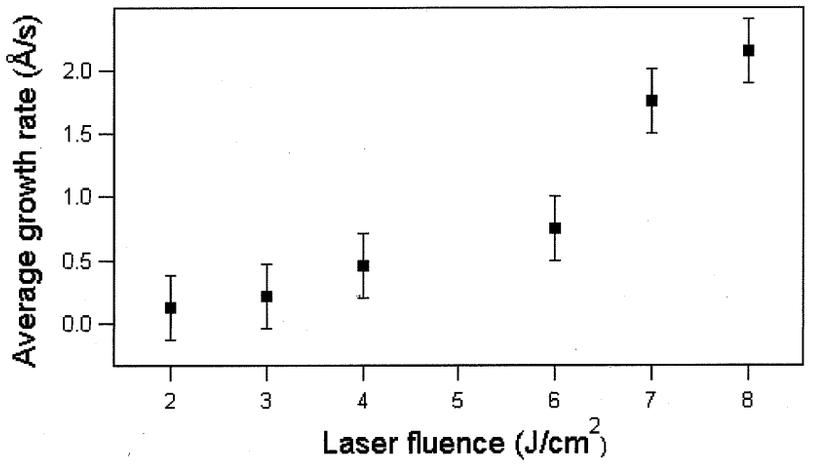

Figure 3. Average growth rate of $La_{0.6}Ca_{0.4}MnO_3$ films for a laser fluence ranging between 2 and 8 Jcm^{-2}.The substrate temperature was 650 °C and 30 000 pulsed were applied.

The elemental composition of the target material determined by Energy Dispersive X-ray analysis (EDX) and Laser Assisted – Inductively Coupled Plasma – Mass Spectrometry (LA-ICP-MS) analysis reveals a nominal composition of the target of $La_{0.6}Ca_{0.4}MnO_3$ (LCMO), which is in agreement with the manufacture specifications (Praxair Surface Technology). The film composition analysis, as evaluated by EDX and RBS/ERDA, indicates deviations in the Ca and O content as compared to the target (see table 1). Deficiencies of light elements, such as O and Ca, in the films grown by PLD may be attributed to the larger angular scattering of the light elements in the plume, as previously observed for Li in $LiMn_2O_4$ [21].

Table 1. Elemental composition of the target and films measured by EDX and RBS/ERDA

Element	Target (EDX)	Thin films (EDX)	Thin films (RBS/ERDA)
La	0.630± 0.050	0.770± 0.050	0.74
Ca	0.365± 0.040	0.235± 0.040	0.28
Mn	0.950± 0.050	0.800± 0.010	1
O	2.950± 0.050	2.700± 0.150	2.77± 0.050

The target to substrate distance (D_{T-S}) is an important growth parameter for PLD. The optimal target to substrate distance corresponds to a regime where the kinetic energy of the species arriving at the substrate allows for sufficient surface diffusion to enable epitaxial growth. The quality of the epitaxial growth is evaluated by measuring the (040) X-ray diffraction peaks of LCMO films and the corresponding full width at half maximum (FWHM). For a substrate temperature of 650 °C and an oxygen background pressure of 10^{-3} mbar, the FWHM of the (040) diffraction peaks obtained at various target to substrate distances are shown in figure 4. The best epitaxial growth is obtained for a target to substrate distance between 4 and 5 cm. Smaller distances from the target (e.g. 3 cm) result in films with poorer crystallinity, which can be primarily attributed to the bombardment of the growing films by a non- thermalized flux of atoms and ions with high kinetic energies. Larger distances from the target result in a reduced deposition rate, and hence seemed to affect the crystallinity of these films. RBS analysis did not indicate significant changes in the stoichiometry of the films as a function of D_{T-S}. However, the as deposited films are found to be oxygen deficient.

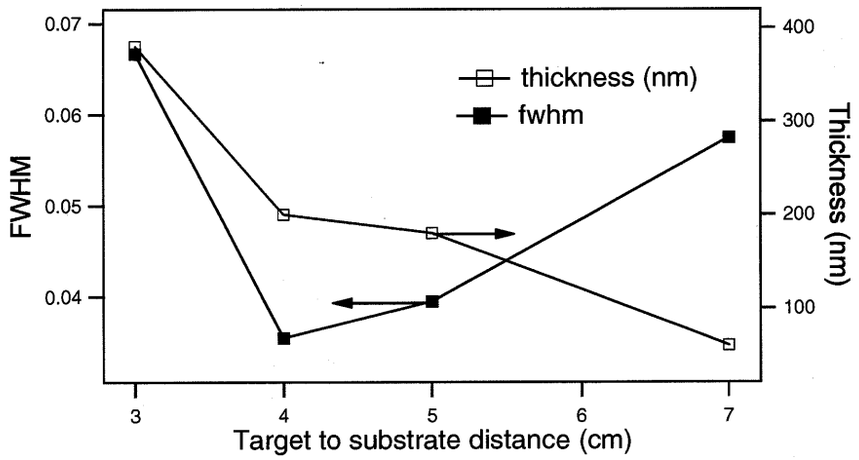

Figure 4. FWHM of the (040) diffraction peak and corresponding films thickness as a function of the target to substrate distance.

The corresponding electrical curves of the LCMO films deposited on $SrTiO_3$ substrates at various distances are shown in figure 5. All films reveal an insulator- like behavior in the measured temperature range between 100 and 300 K. The films grown at distances between 3 and 5 cm exhibit a resistivity value, ρ, at room temperature of 400 μΩcm (close to the bulk material), while the films grown at 7 cm have a bulk resistivity of 100 μΩcm. This suggests that films grown at a target to substrate distance of 7 cm are strained (due to the low deposition rate resulting in a film thickness of 50 nm), while for smaller distances (corresponding to thick layers with a thickness from 240 nm to 440 nm) the strain is released over the films thickness. The mismatch between the substrate and the film induces a tensile strain and therefore a compression of the unit cell in the out of plane direction. This leads to a reduction of the Mn - O - Mn angle, increase of the electron hoping transfer integral and thus a decrease of the bulk resistivity [32].

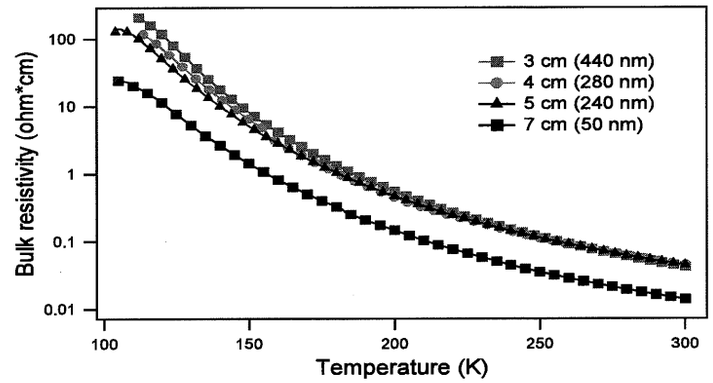

Figure. 5. Electrical transport curves of the films deposited at various target to substrate distances.

The largest magnetoresistance (MR) values were obtained for films grown at a target to substrate distance of 4 cm. Figure 6 shows the resistivity at 0T, 2T and 4T as a function of temperature. The MR ratio, defined as $[\rho(0)-\rho(H)]/\rho(0)$, has a maximum value of 83% at the transition temperature of 120 K in a field of 4 T. This suggests that the films grown epitaxially on the substrate and with a high degree of crystallinity have larger CMR values.

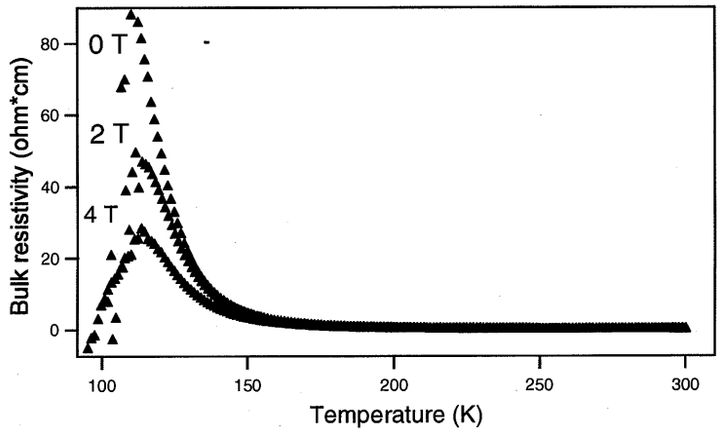

Figure 6. Resistivity versus temperature for a LCMO film deposited at 4 cm measured in different magnetic fields 0T, 2T and 4T.

2.2. Microstructure of $La_{0.7}Ca_{0.3}MnO_3$ Epitaxial Thin Films

The strain induced in thin films due to the lattice to substrate mismatch may cause phase separation and inhomogeneities which yield electrical properties different from those of the bulk. The deformation of the unit cell of $La_{0.7}Ca_{0.3}MnO_3$ grown on $SrTiO_3$ as induced by the substrate lattice mismatch was analyzed using X- ray diffraction (XRD) and high resolution TEM (HTEM). The XRD diffraction pattern of a $La_{0.7}Ca_{0.3}MnO_3$ thin film grown on $SrTiO_3$ is shown in figure 7. The main peaks observed in θ- 2θ scans are (002) and/or (110)

reflections from the film and (200) reflections from the substrate. The inset in figure 7 shows an enlargement of the mentioned features. The double peaks observed in the diffraction pattern are due to the contributions from both $K_{\alpha 1}$ and $K_{\alpha 1}$ lines of the X- ray source.

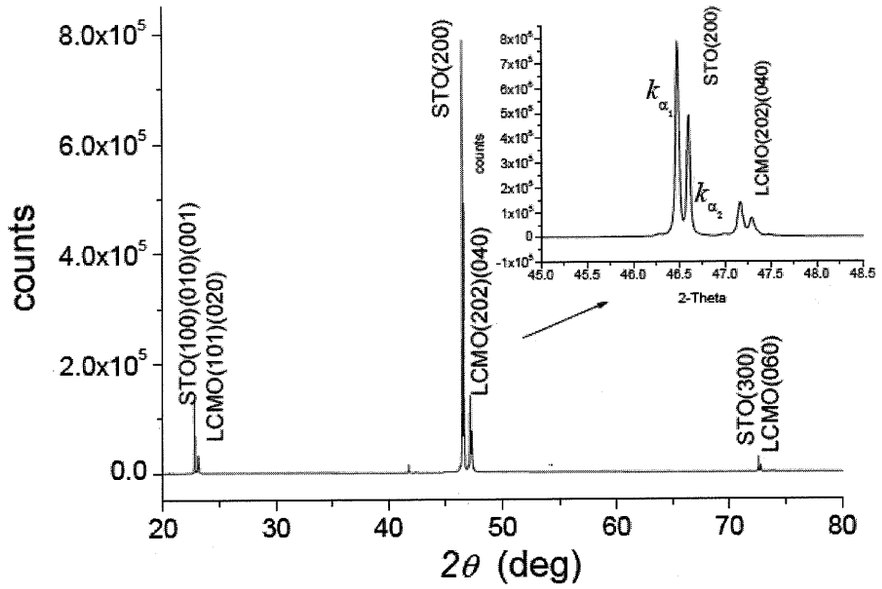

Figure 7. XRD patterns of a $La_{0.7}Ca_{0.3}MnO_3$ thin film grown on $SrTiO_3$.

The cubic Pm3m space group was used for indexing the $SrTiO_3$ substrate, (Code: 01-089-4934), with a= 0.3905 nm, and the orthorhombic space group Pnma was used for indexing the $La_{0.7}Ca_{0.3}MnO_3$ thin film. The X- rays diffraction pattern reveals an orthorhombic distortion, whose lattice parameters are in the following relations with the cubic structure: $a \approx a_p(1/2)^{-2}$, $b \approx 2a_p$, $c \approx a_p(1/2)^{-2}$, a_p= 0.4 nm, where a_p is the lattice of the cubic lattice.

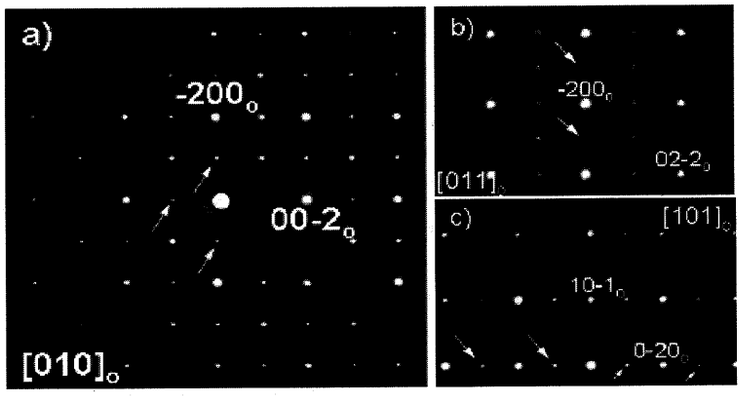

Figure 8. Cross section TEM image of $La_{0.7}Ca_{0.3}MnO_3$ / $SrTiO_3$, b) [100]c $SrTiO_3$ SAED (selected area electron diffraction) pattern, c) $[011]_M$ $La_{0.7}Ca_{0.3}MnO_3$ SAED pattern.

A low magnification TEM image of the cross- sectional structure of the 200 nm LCMO layer grown on the $SrTiO_3$ substrate is shown in figure 8 a. The corresponding diffraction patterns of the substrate (zone axis $[100]_c$ assigned to the cubic structure) and film (monoclinic structure with the $P_{21/c}$ space group) are shown in figure 8 b) and c), respectively.

The cross sectional HREM image of the LCMO film and $SrTiO_3$ substrate is shown in figure 9. The HREM image of the film indicates the presence of twins in the perovskite layer. Different orientations of the c- axis denote the direction of the individual domains within the layer.

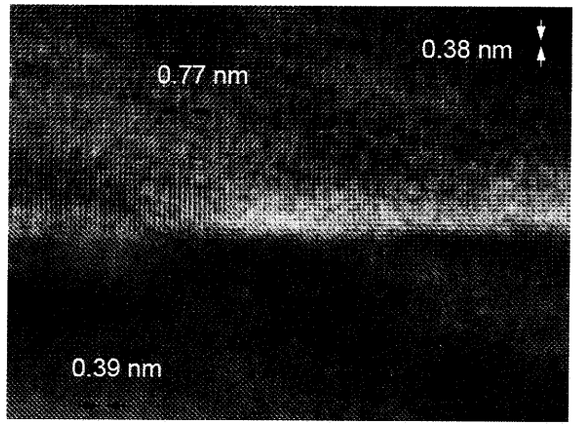

Figure 9. High resolution of the of $La_{0.7}Ca_{0.3}MnO_3$ / $SrTiO_3$ interface in cross section geometry.

It has been suggested, that the twin domains are not necessarily formed during the growth, but that the mixed domains can be formed during the cooling process [22]. The formation of the domains is not completely understood at the moment, but a strong correlation between the strain and domains was found. Previous reports in the literature have shown that for a 5 nm thick $La_{0.7}Ca_{0.3}MnO_3$ layer, only [001] domains are present. When the thickness of the layer is larger than 30 nm, both domains are formed, a consequence of the lattice relaxation. The ratio between the mixed [001]/[110] domains could not be determined, but the majority of the domains are [001]. The LCMO film exhibits an epitaxial growth with a "cube-on-cube" relation with the $SrTiO_3$ substrate. Strain is observed despite the low lattice to substrate mismatch (0.028 %), through misfit dislocations at the interface, which are revealed by the dark/white regions in figure 9.

2.3. Oxygen Vacancies in Manganite Thin Films

Oxygen vacancies can affect dramatically the transport properties of the manganite thin films. Even though the films deposited by Pulsed PRCLA exhibit higher oxygen content as compared to classical PLD [23], the as-deposited manganites are still oxygen deficient, as a consequence, the resulting films have reduced CMR values.

Here we report a systematic study on the effects of annealing treatments on the properties of the manganite films. The films were subjected to various annealing treatments: a) Cooling in O_2 background gas at 50 Pa, followed by an annealing at 400 °C (where oxygen diffusion is considerable) for 1 h, b) moderate annealing in O_2 at 600^0 C for 4 hours, and c) heavy

annealing in an O_2 atmosphere at 900^0 C for 10 hrs at atmospheric pressure. The morphological, structural and transport properties of the resulting films were compared.

The thin films cooled in vacuum have a dark mirror- like appearance, while films with high oxygen content appear dark-blue. In our experiments, some STO substrates were heated in low oxygen atmosphere (8×10^{-2} Pa) and kept for 1 hour before deposition. $SrTiO_3$ has a cubic structure with a lattice constant of 3.905 Å. The $SrTiO_3$ (100) surface can be terminated with a Sr- O plane, or Ti- O plane, and for not specially treated substrates with a mixed surface. The morphology of LCMO films deposited on $SrTiO_3$ depends on whether the substrate was heated or not in an oxygen atmosphere prior deposition. Figure 10 shows AFM scans of LCMO films deposited on STO substrates heated in vacuum and oxygen atmosphere. When the $SrTiO_3$ substrates are heated in vacuum the resulting films have a flat surface, and no clear pattern can be detected. Annealing in an oxygen atmosphere at 700 °C results in a terrace like-structure of the $SrTiO_3$ substrate and therefore of the growing films. This suggests that the thermal treatment of the substrate prior deposition has a pronounced influence on the surface morphology of the growing films.

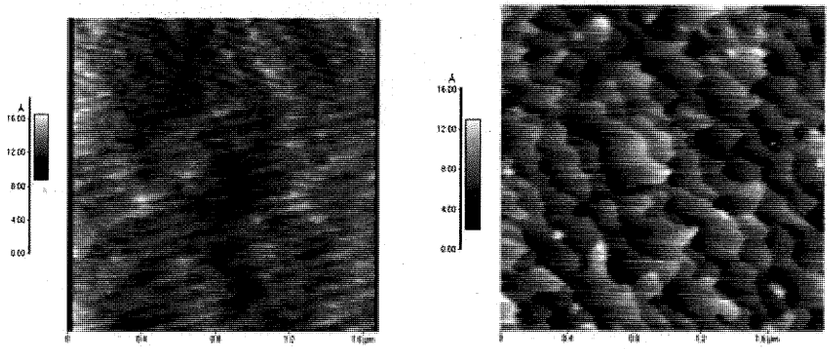

Figure 10. AFM images of LCMO films grown on $SrTiO_3$ substrates which were heated in vacuum (left) and in an oxygen atmosphere (right).

The composition of the LCMO layers as determined by RBS/ERDA is shown in table 2. The data reveal an increase of the oxygen content of the films which were cooled in an oxygen atmosphere as compared with films cooled in vacuum.

Table 2. Elemental composition of the films after post deposition treatments

Elemental composition	Post deposition treatments
$La_{0.75\pm0.03}Ca_{0:25\pm0.01}Mn_{0.88\pm0.03}O_{2.75\pm0:14}$	Cooling in vacuum
$La_{0.7\pm0.03}Ca_{0.3\pm0.01}Mn_{0.88\pm0.03}O_{2.85\pm0.14}$	Cooling in O_2 atmosphere

As expected, an increase of the oxygen content in the films results in an improvement of the electrical properties of the films. The plots of $\ln(\rho/T)$ versus $T^{-1}(K^{-1})$ for the films cooled in vacuum and oxygen are shown in figure 11. The activation energy, E_a, obtained from the slope of the linear dependence is 135 meV for the as deposited films and 128 meV for the

films cooled in an oxygen atmosphere. An increase in the oxygen content results in films with a smaller activation energy and increased CMR values.

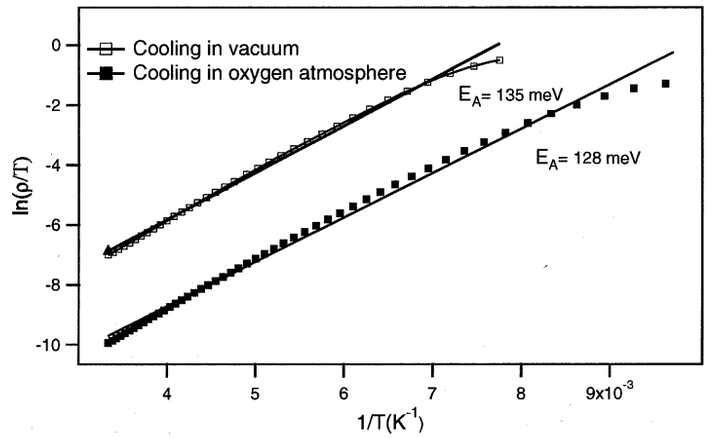

Figure 11. Plots of $\ln(\rho/T)$ vs $T^{-1}(K^{-1})$ for $La_{0.7}Ca_{0.3}MnO_3$ thin films for fast and slow cooling.

When cooling is performed in oxygen, the MR value increases considerably. The change of the bulk resistivity with the applied magnetic field for the film cooled in oxygen is shown in figure 12. At zero field, the film exhibits an insulating behavior, while at 5T a transition from the insulating to the metallic state is induced.

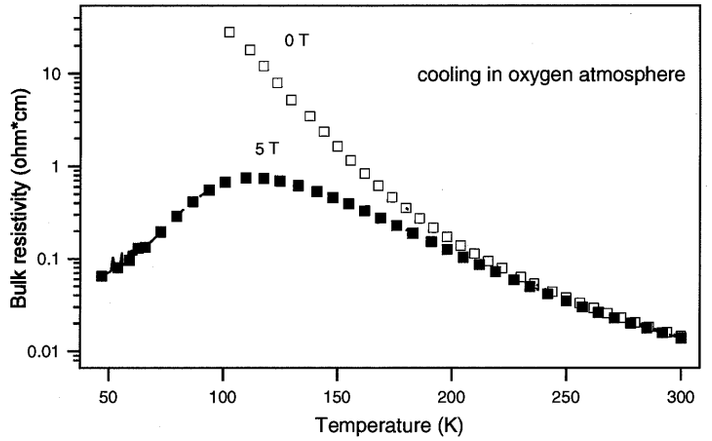

Figure 12. Temperature dependence of the resistivity for a film cooled in O_2 at applied magnetic fields of 0 T and 5 T, respectively.

Heavy annealing (e.g. 900 °C for 10 h and 1 bar O_2 atmosphere) can improve the transport properties of the thin films even further. Figure 13 shows the temperature dependence of the resistivity for the heavily annealed LCMO films at magnetic fields of 0T, 0.5T, 1T, 2T and 5 T. The transition temperature shifts by 4 K towards higher temperatures upon annealing. An increase in the oxygen content can induce changes in the transport properties of the films similar to the ones resulting from an externally applied pressure. The

external pressure induces a lattice contraction which favors the electron transfer probability in the Mn - Mn network, resulting in a shift of the transition temperature to higher values. The maximum magnetoresistance (plotted in the inset of the figure 13) reaches 90% at a magnetic field of 5 T.

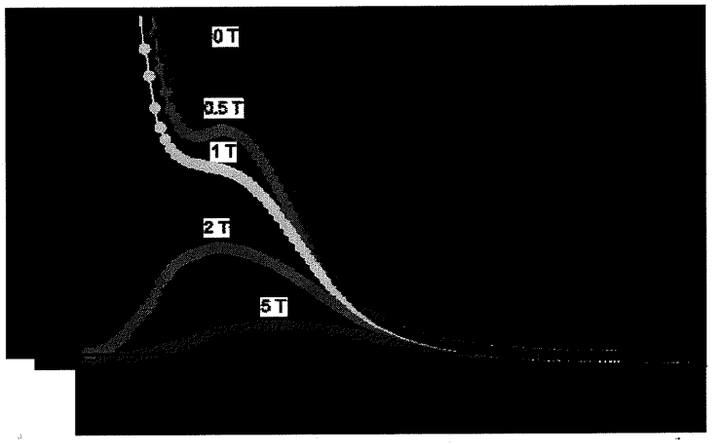

Figure 13. Temperature dependence of the bulk resistivity for a LCMO film heavy annealed at the applied fields of 0 and 5 T, respectively. Inset: The maximum MR at different magnetic fields.

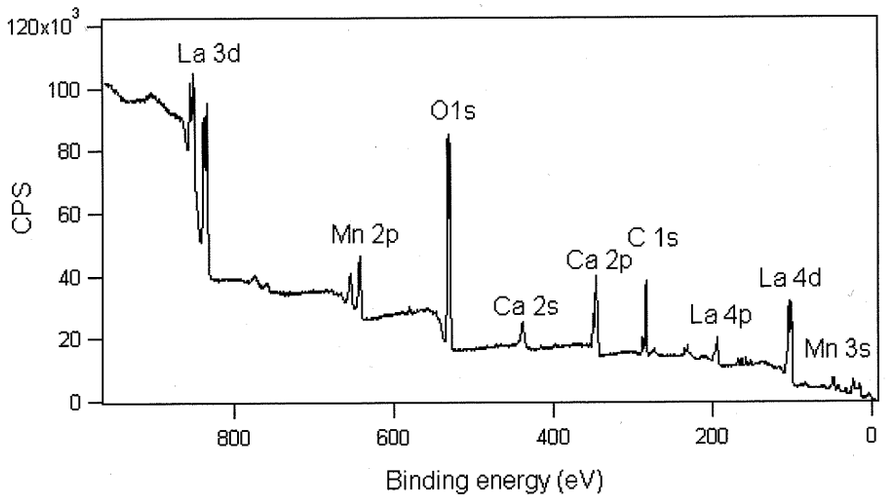

Figure 14: Survey spectra of the annealed $La_{0.7}Ca_{0.3}MnO_3$ thin film's surface.

As the oxygen content influences the oxidation state of the Mn in the unit cell, we attempt to establish a correlation between the Mn^{3+}/Mn^{4+} ratio and the oxygen content which determines the electron transfer in the double exchange mechanism. In this chapter, results from photoemission spectroscopy techniques employed to explore the electronic configuration of the manganite thin films are presented. X-ray photoelectron spectroscopy (XPS) provides information about the surface composition of the $La_{0.7}Ca_{0.3}MnO_3$ manganite thin films (around 2-3 nm), whereas X-ray absorption spectroscopy (XAS) offers information

from the bulk (around 8- 10 microns). XPS measurements were performed without prior surface cleaning treatments. XANES spectra at the Mn K-edges were collected in the fluorescence mode (for thin films) and in the transmission mode (for reference samples).

The XPS survey spectra (figure 14) show the main peaks assigned to the film, i.e. La 3d, Mn 2p, O 1s, Ca 2s, Ca 2p, La 4d, Mn 3s, as well as an intense C 1s peaks due to surface contaminations.

The O 1s core levels of the as deposited/ annealed films reveal the presence of two oxygen species at the surface (see figure 15). The O 1s peak at lower binding energy (528.7 eV- 529 eV) can be assigned to the O^{2-} in the perovskite structure [24], while the peak at the higher binding energy (531.5 eV) can be assigned to the surface contaminants. Similar observations have been reported previously for $La_{0.6}Ca_{0.4}CoO_3$ and have been attributed to $CaCO_3$ species at the surface [25]. The interpretation of the O 1s peaks at the surface of the thin films is difficult due to the surface contaminants. The O 1s peaks, influenced by the stoichiometry of the LCMO perovskite, can be due to the signal from contributions of the Mn- O layer, Ca/La- O containing layer or a mixture of both [26]. A shift of the O 1s peaks towards lower binding energy is observed upon annealing.

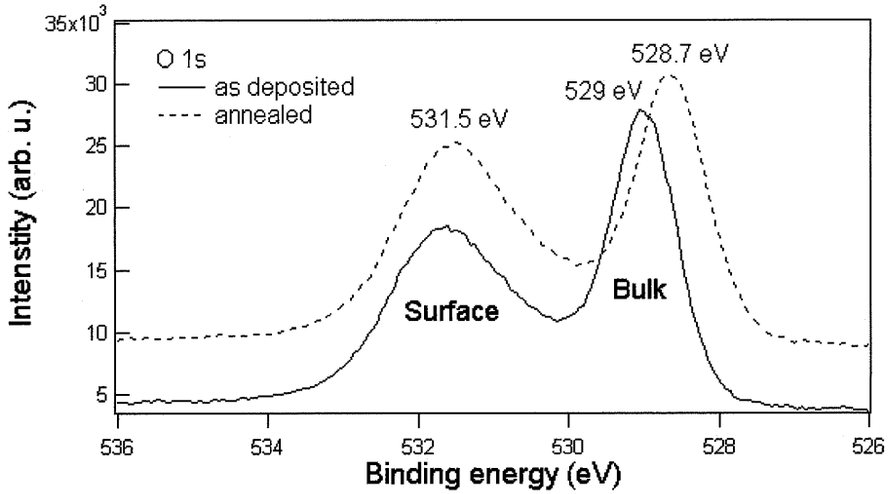

Figure 15. O 1s core level spectra of $La_{0.7}Ca_{0.3}MnO_3$ thin films.

The XPS signal of the Ca 2p core levels, shown in figure 16, originates from two different contributions, e.g. surface contaminants and film. The Ca $2p_{3/2}$ peak has a binding energy of 346 eV (349.26 eV for Ca $2p_{1/2}$) and shifts by 0.36 eV toward lower binding energy after annealing. The binding energy of the Ca 2p component in the $La_{0.7}Ca_{0.3}MnO_3$ thin films is 0.6 eV lower than that observed for $La_{0.9}Ca_{0.1}MnO_3$ [27]. The peak at 347.2 eV can be assigned to the $CaCO_3$ surface species, which is in agreement with the binding energy (BE) of the O 1s peak at 531.5 eV.

As mentioned before, the Mn^{3+}/Mn^{4+} ratio in the manganese perovskites depends strongly on the oxygen content and determines the CMR values. The average Mn valence in the uppermost atomic layers could be determined from the position of the Mn core levels. The $Mn2p_{3/2}$ peaks are broad, originating from the mixture of Mn^{3+} and Mn^{4+} ions present at the sample surface. The different oxidation states of Mn exhibit different values, e.g. binding

energy (MnO_2) = 642.6 eV and binding energy (Mn_2O_3) = 641.9 eV. As the peaks are not well resolved, fitting of the Mn 2p signal cannot be done accurately. It has been shown that by using the multiplet splitting values of the Mn 3s core level, an estimated for the average Mn valence can be made [28]. The Mn 3s core level of the transition metals exhibit an exchange splitting due to the interaction between the 3s hole created by the X- rays photoelectron emission process and 3d electrons of the Mn ion (see figure 17). The parallel or antiparallel alignment results in a splitting of the Mn 3s signal into two peaks. The difference in binding energy of the two peaks is called exchange splitting, and can be reliably used to quantitatively estimate the Mn valence state.

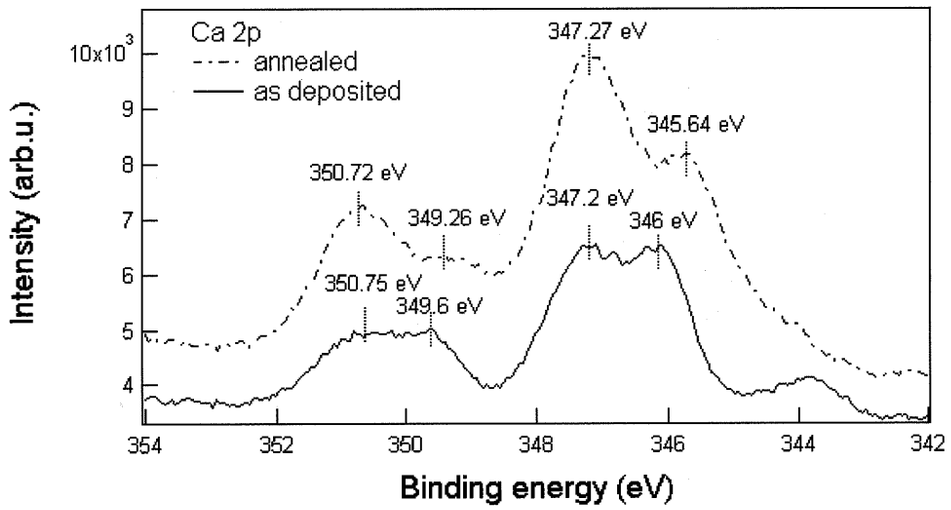

Figure 16. The Ca 2p signals of an as deposited and annealed $La_{0.7}Ca_{0.3}MnO_3$ film.

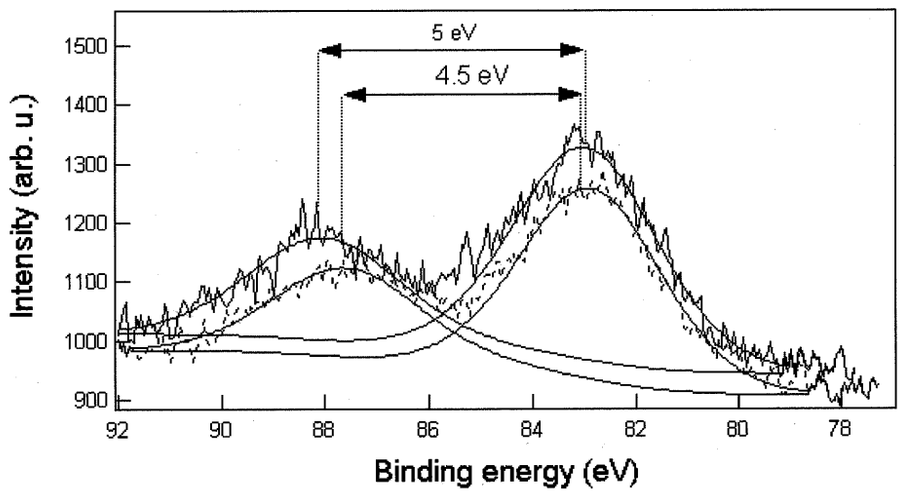

Figure 17. XPS signals from the Mn 3s multiplet splitting of the as-deposited films (continuous line) and annealed at 0.5 mbar O_2 atmosphere (dash-dot line) fitted with Gaussian functions.

The exchange splitting values obtained from the fitting are summarized in table 3. The film stoichiometry determined from RBS/ERDA measurements (included in the same table) reveals a slight increase of the oxygen content upon annealing. The exchange splitting values of the standard samples MnO_2 and Mn_2O_3 are also given. For the as deposited films an exchange splitting value of 5 eV is obtained, indicating that the Mn average valence is in between Mn^{3+} and Mn^{4+}. Annealing in oxygen atmosphere for 1h results in a decrease of the exchange splitting value to 4.7 eV, and after 4 h annealing the splitting decreases to 4.5 eV. This suggests that post-deposition annealing induces a strong oxidation of the manganite surface, and that a layer containing Mn^{4+} species is formed at the surface.

Table 3. Multiplet splitting values of the Mn 3s core level

Material	Stoichiometry (RBS/ERDA)	ΔEs(eV)
$La_{0.6}Ca_{0.4}MnO_3$	$La_{0.75}Ca_{0.25}Mn_{0.88}O_{2.75}$	5 eV
MnO_2	-	4.5 eV
Mn_2O_3	-	5.5. eV

The XPS spectra reveal that all species exhibit the same trend, e.g. shift towards lower binding energy upon annealing, which can be interpreted as an enhancement of the surface metallicity. Whether the observed increase in the Mn oxidation state also occurs in the bulk, was studied by X-ray absorption spectroscopy. Throughout the experiments only the fluorescence detection mode was employed, with an X-ray penetration depth of 8-10 μm, which includes the entire film thickness and part of the $[(LaAlO_3)O_3(Sr_2AlTaO_6)_{0.7}]$ (100) (LSAT) substrate. For a given film thickness, this technique probes the average bulk electronic structure. Figure 18 shows the Mn K-edge spectra of $LaMnO_3$ and $SrMnO_3$ reference compounds in comparison with those of the annealed $La_{0.7}Ca_{0.3}MnO_3$ (red) and as-deposited (blue) thin films. After normalization, an energy shift of the main edge can be observed (as indicated by the arrows in figure 18 which shows the peak position of the first derivative for the corresponding spectrum). The energy shift towards higher energy reveals that the Mn oxidation state changes from +3 in the as-deposited films to +3.4 in the annealed films. A similar energy shift was obtained previously on powder precipitates upon annealing in O_2 atmosphere and it is consistent with Mn^{4+} (t_{2g}) configuration sites [29]. A pre-edge feature around 6540 eV, located approximately 15 to 20 eV below the main K-edge crest of manganese can be observed in figure 18. The pre-edge feature is related to electronic transitions from the 1s core levels to the empty 3d levels which are hybridized with 4p levels through the Mn ligands (thus probing the density of the lowest unoccupied states). The discrepancies in energy position and relative areas between the pre edges of the two films can be attributed to variations in the effective number of 3d electrons in the excited-state configurations. The increased hybridization between the Mn d/p bands which supports an increased fraction of Mn^{4+} (t_{2g}) states can be clearly seen in the pre-edge features of the annealed compared to the as-deposited film.

The data reveal that the surface changes in oxidation states (XPS) can be clearly separated form the bulk contributions (XAS). After O_2 annealing, the films surface has changed, containing mostly Mn^{4+} ions and probably a higher oxygen content, while in bulk the presence of a mixture of Mn^{3+} and Mn^{4+} valence are present. The spectroscopic findings are in good agreement with the resulting transport properties. An increase of the oxygen

content leads to an increase in the Mn^{4+} carriers. More Mn^{3+}- O^{2-}- Mn^{4+} networks available in the perovskite structure the conduction of e_g electrons, reducing the bulk resistivity and increasing the MR values.

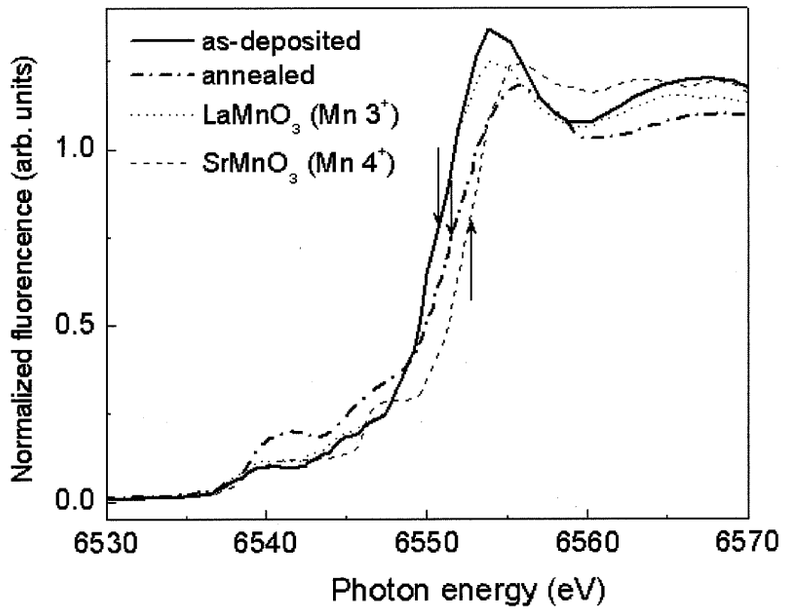

Figure 18: Normalized Mn K-edges of $LaMnO_3$ (Mn^{3+}) (dotted line) and $SrMnO_3$ (Mn^{4+}) (dashed line) reference compounds compared to the annealed $La_{0.7}Ca_{0.3}MnO_3$ (dash dot line) and as-deposited (continuous line) thin films. The arrows indicate the positions of the main edges.

3. Fe DOPED $La_{0.7}Ca_{0.3}Mn_{1-x}Fe_xO_3$ (x=0.2) Thin Films

3.1. Structural, Composition and Electronic Characterization of $La_{0.7}Ca_{0.3}Mn_{0.8}Fe_{0.2}O_3$ Films

Previous studies of the CMR materials have been done through doping of the La sites, which reveals information about the lattice effects, and influences the double exchange (DE) interaction. Although the manganite materials have been widely studied, there have been very few studies in doping the Mn sites, which represent the key of the double exchange interaction (together with the oxygen ions). Ahn et al. [30] have shown that Fe doping (<20%) on the Mn sites in the ferromagnetic (x= 0.37) and the antiferromagnetic (x= 0.53) phases of the $La_{1-x}Ca_xMnO_3$ powders leads to a suppression of the ferromagnetism and conduction.

Here we investigate the role of the Mn^{3+} Jahn- Teller ions on the CMR properties of the manganites, by replacing some of the Mn ions by Fe ions (20%).

Single crystalline materials in the form of thin films were prepared were prepared by PRCLA. In general, the resulting $La_{0.7}Ca_{0.3}Mn_{0.8}Fe_{0.2}O_3$ films have a low surface roughness (RMS= 9Å). The X-ray θ- 2θ scans indicate that the Fe doped LCMO thin films on LAO

substrates are single crystalline (see figure 19). The lattice parameter of the LCMFO films determined form the XRD data is 3.890 Å, which is close to the lattice parameters of the undoped LCMO films, e.g. 3.897 Å. This suggests that Fe substitution in the Mn sites does not induce significant structural changes in the perovskite structure. This is expected, as Fe^{3+} and Mn^{3+} have similar ionic radii, e.g. $r(Fe^{3+})$= 0.645 Å and $r(Mn^{3+})$= 0.64 Å. This is in particular true if we assume that the Fe average valence +3. Our findings are similar with previous literature reports [31].

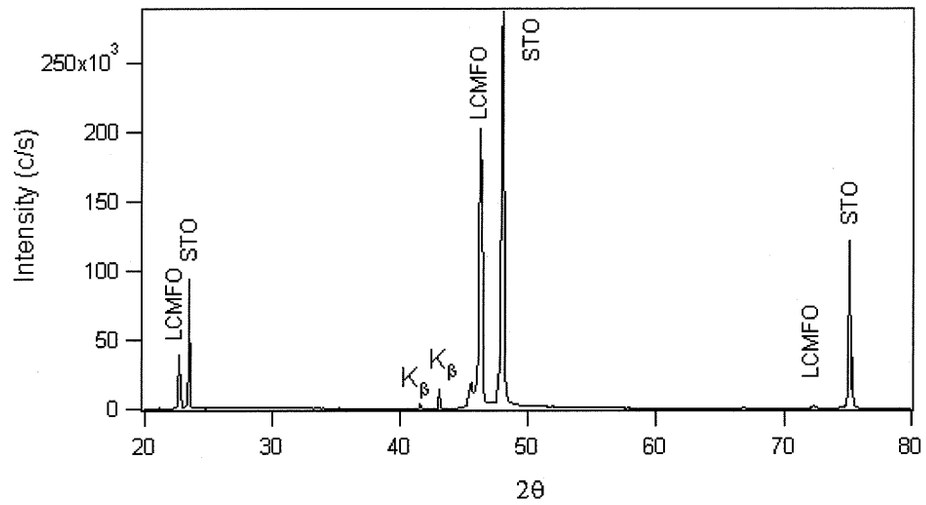

Figure 19: XRD scans of a LCMFO film prepared on $LaAlO_3$ (100).

Mössbauer measurements, carried out on 300 nm thick films, were used to determine the Fe valence state of and its magnetic environment. The results are summarized in table 4 where the term "surface" refers to a probing depth of the film of 150 nm, while the term bulk corresponds to a probing depth larger than 150 nm. The Mössbauer measurements reveal the presence of both Fe^{2+} and Fe^{3+} valence states at the "surface", while in the bulk only Fe^{3+} is detected (4% is within the error bars). However, Fe is found mainly in an oxidation state of +3. The low amount of Fe doping (20%) did not allow an accurate fitting of the Mössbauer spectra. It could therefore not be determined if Fe is coupled ferromagnetically or antiferromagnetically to the Mn- O lattice. Fe was found in an amount of 43% (or 35% in bulk) in a phase whose magnetic character could not be determined (ferromagnetic or antiferromagnetic phase). Similar Mössbauer investigations on materials with a larger Fe doping have shown that the magnetic moments of Fe^{3+} are coupled antiferromagnetically to the ferromagnetic Mn- O lattice [32].

The elemental composition of the $La_{0.7}Ca_{0.3}Mn_{0.8}Fe_{0.2}O_3$ films was investigated using three complementary methods, i.e. RBS, ERDA and PIXE. The RBS method can provide accurate information about the La, Ca, Mn and Fe content with an error of 3 %, while ERDA is used to determine the oxygen content with the same accuracy. The elemental composition of the LCMO films and Fe doped LCMO films analyzed by RBS/ERDA analysis reveals the same oxygen content, confirming thus that Fe ion substitutes the Mn ion without affecting the oxygen content.

Table 4. Fe valence states of the as deposited $La_{0.7}Ca_{0.3}Mn_{0.8}Fe_{0.2}O_3$ films

Material	Probing depth	Fe^{3+}[%]	Fe^{3+}[%]	Phase [1][%]
$La_{0.7}Ca_{0.3}Mn_{0.8}Fe_{0.2}O_3$ on $LaAlO_3$	"Surface"(150 nm)	32	25	43
	"Bulk"(>150 nm)	61	4	35

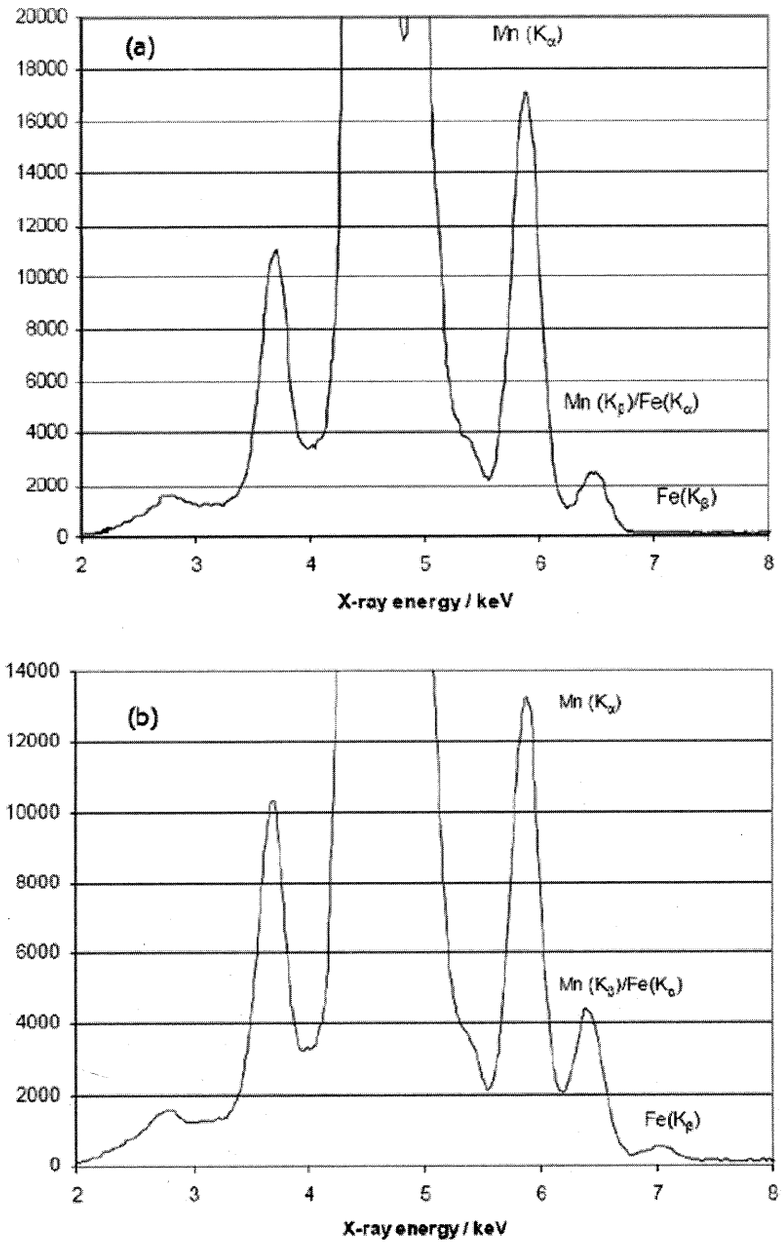

Figure 20. PIXE spectra of the (a) LCMO films and (b) Fe doped LCMO films.

[1] Fe can be found in a ferromagnetic or antiferromagnetic phase.

A quantitative separation of Mn from Fe was not possible due to the low mass resolution of RBS. Photon Induced X- ray Emission (PIXE) technique was employed instead to determine the Fe content. The corresponding PIXE spectra are shown in figure 20. The estimated Fe/Mn ratio from the K_β (%) peak area is 25 % (±3%) for LCMFO films and is smaller than 1.4 % (which is in the measurements errors) for the undoped samples. The PIXE analysis indicates that a congruent transfer of Fe (20 ±3 %) is achieved by PRCLA.

With Fe doping, the bulk resistivity of the manganite thin films increases dramatically. The ratio of bulk resistivity of x= 0.2 with respect to x= 0 is: $\rho(x=0.2)/\rho(x=0) \sim 9$. Fe doping induces therefore an increase by almost one order of magnitude of the bulk resistivity at room temperature. The activation energy increases upon Fe doping. The activation energy was determined from the polaron conduction equation; fittings of $\ln(\rho/T)$ vs $1000/T(K^{-1})$ for the $La_{0.7}Ca_{0.3}Mn_{1-x}Fe_xO_3$ samples with x=0 and 0.2 are shown in figure 21. The obtained activation energy is shown in the same figure. Fe doping in the LCMO compounds induces an increase of the activation energy from 100 meV for LCMO samples to 154 meV for the LCMFO samples. The increase in the activation energy suggests that the hopping mechanism is reduced. Furthermore, the CMR value is considerably reduced upon Fe doping. Fe is found invariably in the valence state +3 (mainly), and a direct substitution of Mn^{3+} by Fe^{3+} is most probable. Each Fe^{3+} ion substituting a Mn^{3+} ion will perturb the long order ferromagnetic interaction, weakening therefore the double exchange mechanism; as a consequence the CMR effect is reduced. It is therefore important to study the electronic configuration of the Mn and Fe ions in order to correlate the results with the transport properties of the film.

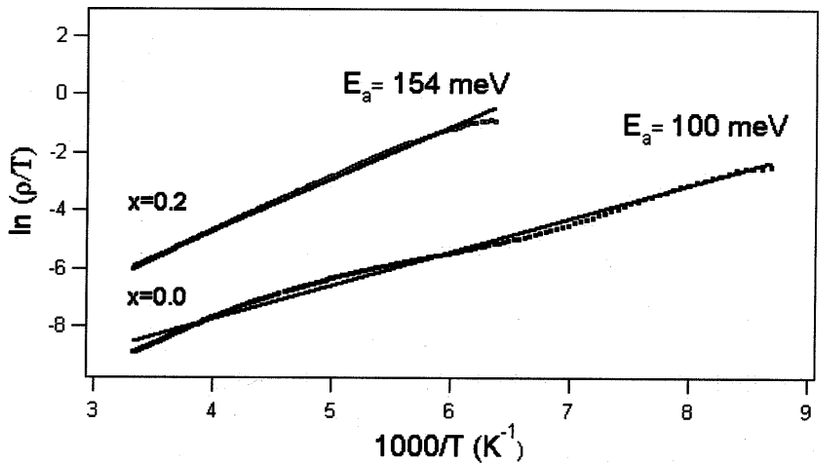

Figure 21. Plots of $\ln(\rho/T)$ vs $1000/T(K^{-1})$ of $La_{0.7}Ca_{0.3}Mn_{1-x}Fe_xO_3$ (x=0 and x= 0.2).

3.2. Electronic Properties of the Fe (20%) Doped $La_{0.7}Ca_{0.3}Mn_{1-x}Fe_xO_3$ Thin Films

Near edge and X-ray absorption spectroscopy measurements were carried out to probe the configuration of Mn and Fe, as well as changes in the chemical state of the elements. A comparison between the Mn K edge spectra of the $La_{0.7}Ca_{0.3}Mn_{1-x}Fe_xO_3$ films, with (x=0 and

0.2), is given in figure 22. No change in the main K edge position was observed, suggesting that the predominant Mn valence does not change upon Fe doping. The main difference between the annealed and not annealed films consists in the intensity drop of the main feature at the Mn K-edge. The feature can be associated with disorder induced in the perovskite lattice due to the high oxygen deficiencies and different valence states of Fe and Mn.

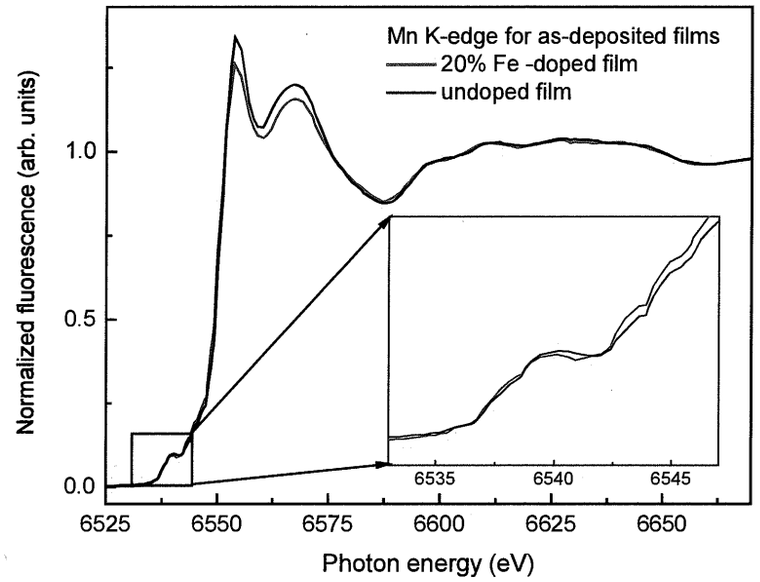

Figure 22. Normalized Mn K-edges of $La_{0.7}Ca_{0.3}Mn_{1-x}Fe_xO_3$ (x=0, 0.2) as-deposited films grown on $[(LaAlO_3)O_3(Sr_2AlTaO_6)_{0.7}]$ (100) substrates. The inset shows an enlargement of the pre-edge region.

The Mn K-edge spectra of the annealed $La_{0.7}Ca_{0.3}Mn_{1-x}Fe_xO_3$ (x = 0, 0.2) films is shown in figure 23. After annealing, the main absorption line of the LCMO and Fe doped LCMO shows the same intensity, but a change in the pre-edge features is observed. The pre-edge region enlarged in the inset of figure 23 is related with transitions into final d- states, e.g. electronic transitions from 1s into empty d states or hybridized d/p states [33]. The Mn pre-edge features for the doped film reveal an increase in the a_1 feature intensity relative to the a_2 feature. Simple crystal field theory suggests an association of the first feature (a_1) with the e_g majority spin states and of the feature at higher energy (a_2) with t_{2g} and e_g spin states. The increase in the a_1 feature with respect to the a_2 feature reveals an increased localization of the Mn 3d- orbitals after Fe substitution for the annealed films. The lattice disorder observed in the as-deposited films can be related to the high oxygen deficiencies.

Near Edge X- ray Absorption Spectroscopy (NEXAS) studies were employed to determine the Fe valence state in the bulk and the density of the unoccupied states. For comparison, a Fe_2O_3 powder (Fe^{3+}) reference compound is shown together with the Fe K-edge spectra of the annealed and not-annealed LCMFO films in figure 24. The position of the inflection point, indicated by an arrow was determined as the point where the slope is maximum. The edge region indicates that the average valence of Fe is between +2 and +3, which is in agreement with the Mössbauer measurements. The bimodal distribution of the pre-edge (features b_1 and b_2) in the annealed films compared with the not-annealed films

gives some evidence of Fe- site localization effects, but it is not possible at the moment to associate these features with specific d-states.

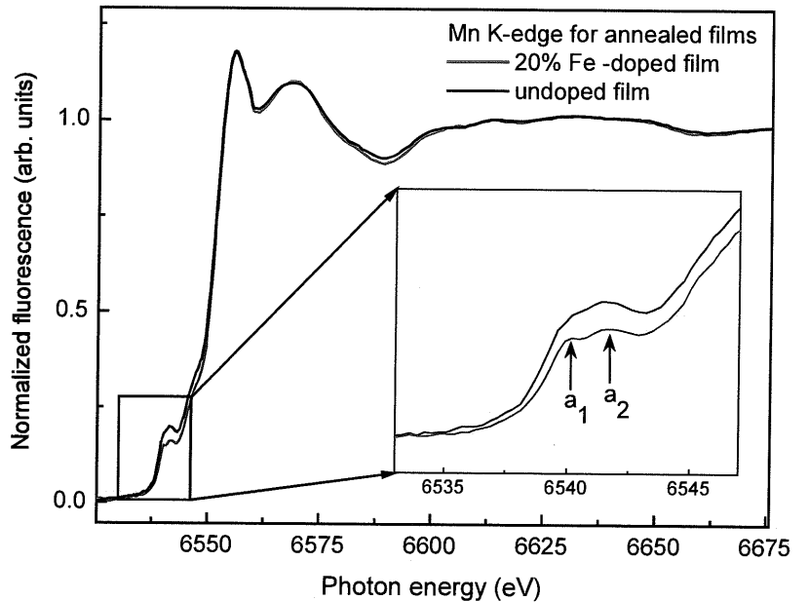

Figure 23. Normalized Mn K-edge of $La_{0.7}Ca_{0.3}Mn_{1-x}Fe_xO_3$ (x=0, 0.2) annealed thin films grown on LSAT. The inset shows an enlargement of the pre-edge region.

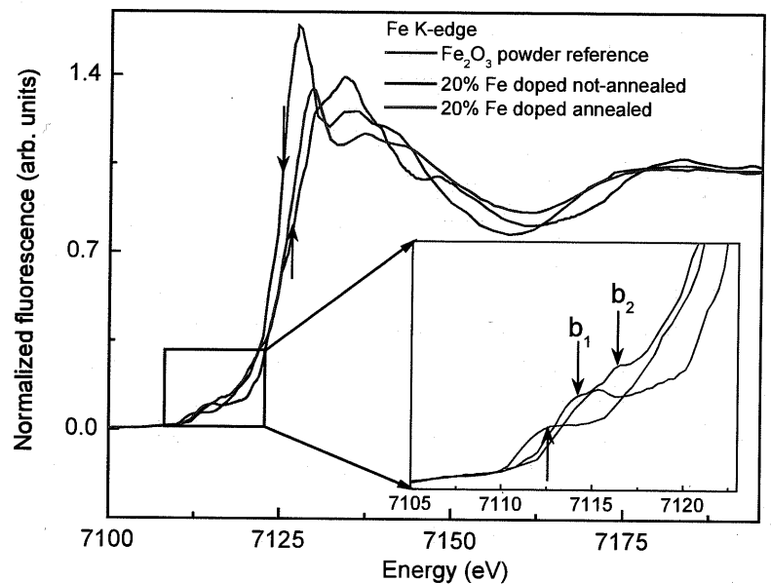

Figure 24. Normalized Fe K-edges of Fe_2O_3 (Fe^{3+}) powder reference, as well as of $La_{0.7}Ca_{0.3}Mn_{0.8}Fe_{0.2}O_3$ annealed and not-annealed films. The arrows indicate the positions of the edges. The inset shows an enlargement of the pre-edges features.

The increase of the polaron activation energy is associated with the increase of Mn ion orbitals localization upon Fe doping in the LCMO films. Our findings have also to be correlated to the literature data. Calculations of the electronic band in Fe doped compounds have shown that the top of the Fe e_g band is almost located at the bottom of the Mn e_g band, just with an overlap of less than 3%. Fe^{3+} ions replacing Mn^{3+} ions do not favor the hopping of the carriers towards Mn^{4+} ions, acting therefore as trap centers of the double exchange mechanism [30]. As a consequence, the partial substitution of the Mn ions by the Fe ions suppresses of the double exchange interaction and reduces the magnetoresistance.

Conclusion

In summary, we report on properties of magnetic manganite thin films grown by pulsed reactive crossed beam laser ablation. The influence of the PLD parameters, such as laser fluence, target to substrate distance, and post- annealing treatments, on the crystallography, composition, morphology and transport properties of the films was studied. The films deposited in a wide fluence range, i.e. 2 Jcm^{-2} to 8 Jcm^{-2}, have a similar elemental composition, but Ca and O deficiencies were observed. The RBS results reveal that films with the composition of $La_{0.7}Ca_{0.3}MnO_{3\pm\delta}$ are obtained from a target with a composition of $La_{0.6}Ca_{0.4}MnO_3$

A high epitaxial quality results in a high colossal magnetoresistance (CMR) value. High oxygen deficiencies in the growing films lead to a dramatic reduction of the colossal magnetoresistance (CMR) ratio. Oxygen acts as a bridge between the Mn^{3+} and Mn^{4+} ions and has therefore a pronounced influence on the double exchange interaction which is the main mechanism for the CMR. The films cooled in vacuum have the highest oxygen deficiencies and therefore the lowest magnetoresistance ratio, while the films cooled in oxygen atmosphere have a higher oxygen content resulting in a larger magnetoresistance. Further annealing after deposition at high temperatures can improve the magnetoresistance even more.

Changes in the oxidation states of the Mn species induced by the oxygen vacancies were probed by XPS (surface sensitive) and XAS (bulk sensitive). Higher oxygen content leads to an increase in the oxidation states of the Mn species, and thus to an increase of the Mn^{4+} species. This favors the hopping of electrons in the Mn^{3+}-O^{2-}-Mn^{4+} network, which increases the electrical conductivity and the magnetoresistance.

The hopping mechanism in the Mn^{3+}-O^{2-}-Mn^{4+} network was tested by replacing part of the Mn ions with Fe ions. The as deposited films exhibit mixed valence states of Fe^{2+} and Fe^{3+}, inducing disorder in the perovskite structure. After annealing, only Fe^{3+} was detected. The XAS data shows a localization of the Mn 3d orbitals after Fe doping, suggesting that the Fe ions act as trapping centers for the electrons exchange. The resulting Fe doped films exhibit a large bulk resistivity and a reduced CMR. This suggests that the mixed valence states of Mn^{3+} and Mn^{4+} is important for maximizing CMR effect.

Acknowledgments

We would like to thank Myriam Aguirre for many useful discussions and C.W. Schneider for critical reading of the manuscript. Special thanks to Anke Weidenkaff and Myriam Aguirre for help with the XRD and TEM measurements. Swiss National Science Foundation is gratefully acknowledged.

References

[1] Baibich, M. N.; Broto, J. M.; Fert, A.; Van Dau, F.; Petro, F. N.; Eitenne, P.; Creuzet, G.; Friederich, A.; Chazelas, J. *Phys. Rev. Lett.* 1988, 61(21), 2472-2475.
[2] Von Helmolt, R.; Wecker, J.; Holzapfel, B.; Schultz, L.; Samwer, K. *Phys. Rev. Lett.* 1993, 71(14), 2331- 2333.
[3] McCormack, M.; Jin, S.; Tiefel, T.H.; Fleming, R. M.; Phillips, J. M.; Ramesh, R. *Appl. Phys. Lett.* 1994, 64(22), 3045- 3047.
[4] Wollan, E.O.; Koehler, W. C. *Phys. Rev.* 1955, 100(2), 545- 563.
[5] Anderson, W.; Hasegawa, H. *Phys. Rev.* 1955, 100(2), 675- 681.
[6] Zener, C. *Phys Rev* 1951, 82(3), 403- 405.
[7] Millis, A. J.; Littlewood, P.B.; Shraiman, B.I. *Phys. Rev. Lett.* 1995, 74(25), 5144- 5147.
[8] Ahn, K.H.; Wu, X.W.; Liu, K.; Chien, C.L. *Phys. Rev. B* 1995, 54(21), 15299- 15302.
[9] Morimoto, Y.; Asamitsu, A.; Kuwahara, H.; Tokura, Y. *Nature.* 1996, 380, 141-144.
[10] Fawcett, I.D.; Veith, G.M.; Greenblatt, M.; Croft, M.; Nowik, I. *Sol. State Sci.* 2000, 2, 821-831.
[11] Gommert, E.; Cerva, H.; Rucki, A.; Helmolt, R. V.; Wecker, J.; Kuhrt, C.; Samwer, K. *J. Appl. Phys.* 1997, 81(8), 5496- 5498.
[12] Min, B. C.; Choi, Y. H.; Moon, S. H.; Lee, S. M.; Lee, S. Y.; Oh B. *Supercond. Sci. Technol.* 2001, 14(8), 543- 547.
[13] Mitu, B.; Bilkova, P.; Marotta, V.; Orlando, S.; Santagata, A. *Appl. Surf. Sci.* 2004, 247(1-4), 123-127.
[14] Voevodin, A.A.; Capano, M.A.; Safriet, A.J. ; Donley, M.S.; Zabinski, J.S. *Appl. Phys. Lett.* 1996, 69(2), 188- 190.
[15] Singh, R.; Paily, R.; Das Gupta, A.; Das Gupta, N.; Misra, P.; Kukreja, L. M. *Semicond. Sci. Technol.* 2005, 20(1), 38- 43.
[16] Satoh, I.; Kobayashi, T.; Katayama, K.; Okada, T.; Itoh, T. *Appl Phys A: Mater Sci. Process.* 2004, 79(4-6), 1445- 1447.
[17] Willmott, P. R.; Huber, J. R. *Rev. Mod. Phys.* 2000, 72(1), 315-328.
[18] Koubaa, M.; Haghiri-Gosnet, A.M.; Desfeux, R.; Lecoeur, P.; Prellier, W.; Mercey, B. *J. Appl. Phys.* 2003, 93(9), 5227- 5235.
[19] Zhang W.; Wang, X.; Boyd, I.W. *Appl. Phys. Lett.* 1998, 73(19), 2745-2747.
[20] Van de Riet, E.; Kools, J.; Dieleman, J. *J. Appl. Phys.* 1993, 73(12), 8290- 8296.
[21] Dumont, T.; Lippert, T.; Döbeli, M.; Grimmer, H.; Ufheil, J. ; Novak, P.; Wursig, A.; Vogt, U.; Wokaun A. *Appl. Surf. Sci.* 2006, 252(13), 4902- 4906.
[22] Lu, C. J.; Wang, Z. L.; Kwon, C.; Jia, Q. X. *J. Appl. Phys.* 2000, 88(7), 4032- 4043.
[23] Nath, T.K.; Rao, R. A.; Lavric, D.; Eom, C.B.; Wu, L.; Tsui, F. *Appl. Phys. Lett.* 1995, 30(22), 3294- 3296.

[24] Lee, J. C.; You, D. G.; Le, S. Y.; Sung, M. C.; Song, H. S.; Park, H. S.; Lee, S. H.; Kang, S. K., Jeong, K.; Kim, S.J.; Kim, C.S. *J. Appl. Phys.* 91(1), 221- 224.
[25] Montenegro, M.J.; Döbeli, M.; Lippert, T.; Muller, S.; Weidenkaff, A.; Willmott, P.R.; Wokaun, A. *Thin Solid Films.* 2004, 453-454, 182- 186.
[26] Choi, J.; Zhang, J.; Liou, S.H.; Dowben, P.A.; Plummer, E.W. *Phys. Rev. B.* 1999, 59(20), 13453- 13459.
[27] Delichere, P.N.; Batis, H.; Batis, H. *Appl. Catal. A.* 2005, 282, 173- 177.
[28] Beyreuther, E.; Grafstrom, S.; Eng, L.M.; Thiele, C.; Dorr, K. *Phys. Rev. B.* 2006, 73(15),155425- 155430.
[29] Croft, M.; Sills, D.; Greenblatt, M.; Lee, C.; Ramanujachary, K. V.; Cheong, S.W.; Tran, D. *Phys. Rev. B* 1997, 55(14), 8726- 8732.
[30] Ahn, K.H.; Wu, X.W.; Liu, K.; Chien, C.L. *Phys Rev B* 1995, 54(21), 15299- 15302.
[31] Cai, J.W.; Wang, C.; Shen, B.G.; Zhao, J.G.; Zhan, W.S. *Appl. Phys. Lett.* 1997, 71(12),1727-1729.
[32] Battle, P.D.; Branford, W.R.; Mihut, A.; Rosseinsky, M.J.; Singleton, J.; Sloan, J.; Spring L.E., Vente, J.F. *Chem. Mater.* 1999, 11(3), 674- 683.
[33] Fawcett, I.D.; Veith, G.M.; Greenblatt, M.; Croft, M.; Nowik, I. *Solid State Sci.* 2000, 2, 821- 831.